Cancer Immunology, Immunotherapy (2019) 68:1429–1441
https://doi.org/10.1007/s00262-019-02379-9

ORIGINAL ARTICLE

A VEGFR2–MICA bispecific antibody activates tumor-infiltrating lymphocytes and exhibits potent anti-tumor efficacy in mice

Yao Xu[1,2] · Xinrong Zhang[1] · Yong Wang[2] · Mingzhu Pan[1] · Min Wang[1] · Juan Zhang[1]

Received: 18 December 2018 / Accepted: 11 August 2019 / Published online: 19 August 2019

Abstract

MHC class I-related chain A (MICA) is one of the major ligands for natural killer group 2 member D (NKG2D), which is an activating NK receptor. MICA is expressed on the surface of human epithelial tumor cells, and its shedding from tumor cells leads to immunosuppression. To activate immune response in the tumor microenvironment, we designed an anti-VEGFR2–MICA bispecific antibody (JZC01), consisting of MICA and an anti-VEGFR2 single chain antibody fragment (JZC00) and explored its potential anti-tumor activity. JZC01 targeted vascular endothelial growth factor receptor 2 (VEGFR2) and inhibited tumorigenesis by blocking the VEGFR2 signaling pathway. Additionally, JZC01 promoted NK and $CD8^+$ T cells to release IFN-γ and engaged activated lymphocytes to lysis of VEGFR2-expressing tumor cells. The in vivo anti-tumor activity of JZC01 was investigated by establishing a Lewis lung cancer cell-transplanted mouse model. It effectively reduced the tumor vascular density and increased the infiltration and activation of NK and $CD8^+$ T cells in the tumor microenvironment. Thus, JZC01 functions in anti-tumor angiogenesis and anti-tumor immune activation, and showed improved anti-tumor efficacy combined with docetaxel, which provides a new insight into anti-tumor therapy.

Keywords Cancer immunotherapy · Bispecific antibody · Tumor-infiltrating lymphocyte · VEGFR2

Abbreviations

JZC00	Anti-VEGFR2 single chain antibody
JZC01	Anti-VEGFR2–MICA bispecific antibody
MICA	MHC class I-related chain A
NKG2D	Natural killer group 2 member D
NSCLC	Non-small cell lung cancer
rMICA	Recombined human MICA
rNKG2D	Recombined human NKG2D
TIL	Tumor-infiltrating lymphocytes
VEGF	Vascular endothelial growth factor
VEGFR2	Vascular endothelial growth factor receptor 2

Electronic supplementary material The online version of this article (https://doi.org/10.1007/s00262-019-02379-9) contains supplementary material, which is available to authorized users.

✉ Juan Zhang
zhangjuan@cpu.edu.cn

[1] Antibody Engineering Laboratory, State Key Laboratory of Natural Medicines, School of Life Science and Technology, China Pharmaceutical University, 154#, Tong Jia Xiang 24, Nanjing 210009, People's Republic of China

[2] Sanhome-CPU Joint Laboratory, China Pharmaceutical University, Nanjing 210009, People's Republic of China

Introduction

The immune checkpoint blockade has revolutionized the treatment of cancer; however, only some patients respond to the current checkpoint therapies, suggesting that additional mechanisms underlie tumor immunosuppression [1]. Shedding of MICA is one of the mechanisms of tumor immunosuppression [2]. MICA is rarely expressed on normal cells, but can be induced on damaged, infected, or malignant cells [3, 4]. Cells that express MICA may provide a signal of disorder, which triggers immune cells to serve as a scavenger [5]. NKG2D is the key receptor of MICA and expresses in human NK, activated $CD8^+$ T cells, and γδ-TCR^+ T cells; it modulates innate immune responses and antigen-specific T cell responses [6, 7]. NKG2D-dependent activation on NK cells mediates cell cytotoxicity directly and overrides inhibitory signals delivered by major histocompatibility complex class I molecules. Engagement of the NKG2D receptor provides a co-stimulatory signal for $CD8^+$ T cells in a signal transducer and the activator of transcription 3 (STAT3) in a phosphorylation-dependent manner [8]. However, advanced tumors frequently escape this immune surveillance by proteolytic shedding of MICA through several proteases [9, 10]. High

concentrations of soluble MICA in serum are associated with disease progression in many cancers, which include prostate cancer, neuroblastoma, kidney cancer, multiple myeloma, non-small cell lung cancer (NSCLC) and chronic lymphocytic leukemia [11–17].

In NSCLC patients, high expression of MICA is a predictive factor for poor prognosis [18, 19]. Tumors secrete soluble MICA that binds to NKG2D and down-regulates NKG2D expression on the cell surface, which leads to the loss of the NK/T cell activation trigger [17, 20]. A combination of anti-angiogenesis and anti-tumor immunotherapy demonstrated significant survival benefit in NSCLC patients, which indicates the role of anti-angiogenesis in the treatment of NSCLC (NCT02366143). Tumor angiogenesis is driven principally by interactions between vascular endothelial growth factors (VEGFs) and its primary receptors VEGFR2 [21, 22]. Anti-angiogenic drugs, such as bevacizumab and ramucirumab [23], are used in the clinical treatment for many solid cancers. However, available clinical data show that the improvement in overall survival is modest, and patients acquire resistance during the treatment [24, 25]. One of the possible explanations for resistance to anti-VEGF therapy is immunosuppression. Growing evidence suggests that solid tumors treated with a high-dose anti-angiogenic agent are infiltrated with immunosuppressive innate cells, such as tumor-associated macrophages (TAMs) or myeloid-derived suppressor cells (MDSCs) [26, 27]. However, several preclinical studies also suggest that anti-angiogenic therapy improves tumor-infiltrating T cells [28, 29]. The effects of anti-angiogenic therapy on the immune cells of the tumor microenvironment are diverse. Thus, there is the prospect of finding a driving agent that tends to improve and to activate tumor-infiltrating lymphocytes (TIL) during anti-angiogenic therapy.

In a previous study, we screened a single chain antibody JZC00 by phage display. JZC00 targeted VEGFR2 and blocked the interaction between VEGFR2 and VEGF [30, 31]. To improve the anti-tumor effect, we designed a bispecific antibody JZC01 that consisted of IZC00 and the extracellular domains of human MICA, and we described the in vitro anti-tumor, angiogenic activity in a pilot study [32]. However, a deeper understanding of the immune activation of the MICA fusion antibody is needed. MICA is the main ligand of NKG2D, and although only primates have MICA and MICB genes, human MICA can be recognized by the murine NKG2D receptor [33]. The activation of NK cells in mice by MICA bispecific antibodies has been confirmed [34], but the activation of T cells in mice has not been studied. In this case, we aimed to evaluate the immune activation of MICA bispecific antibodies with immune-competent mice. Our results showed that JZC01 recruited activated NK and $CD8^+$ T cells to the tumor microenvironment and increased the percentage of lymphocytes that were infiltrated, which resulted in significantly increased anti-tumor efficacy in tumor-bearing mouse models.

Cell culture and materials

Mouse Lewis lung carcinoma (LLC) and mouse forestomach gastric carcinoma (MFC) cells were cultured in RPM1640 that contained 10% (v/v) fetal bovine serum. NK92 cells were cultured in Alpha Minimum Essential medium with 2 mM L glutamine, 1.5 g/l sodium bicarbonate, 0.2 mM inositol, 0.1 mM 2-mercaptoethanol, 0.02 mM folic acid, and 100–200 U/ml IL-2. The isolated human $CD8^+$ T cells were cultured in RPMI 1640 that contained 10% fetal bovine serum, anti-CD3 Dynabeads™ (Thermo Fisher Scientific), and 1 μg/ml human CD80-hFc (Sino Biological). The isolated human NK cells were cultured in RPMI 1640 medium that contained 10% fetal bovine serum supplemented with 10 ng/ml recombinant human IL-12 and 10 ng/ml human IL-15 (Sino Biological, China). All cells were incubated in a humid atmosphere of 5% CO_2 at 37 °C. Mouse anti-his antibody was purchased from SunBio Technology (Nanjing, China) and mouse anti-human MICA antibody was purchased from MBL Life Science (Tokyo, Japan). Recombined human MICA (rMICA) was purchased from Sino Biological (Beijing, China). DC101, an anti-mouse VEGFR2 antibody, was purchased from BioXCell (West Lebanon, NH, USA). Recombined human NKG2D (rNKG2D), human VEGFR2, and mouse VEGFR2 were purchased from Novoprotein (Shanghai, China).

Generation and identification of JZC01

The cDNA sequences of JZC00 and human MICA extracellular domain (residues 24–307, identifier: Q29983-1) were integrated into expression vector pPICZαA for JZC01 expression (Fig. 1a) and expressed in *Pichia pastoris* X-33. The clone with high expression of JZC01 was cultured in YPD liquid medium (50 μg/mL zeocin), and then it was inoculated overnight at 30 °C in BMGY (buffered glycerol-complex medium) medium that contained 0.5% glycerol. The cell culture was collected by centrifugation at 3000×*g* for 5 min and resuspended in 5% (v/v) methanol supplemented with BMMY medium (buffered methanol-complex medium), followed by 5 days of fermentation. Finally, the supernatant in the culture was collected. JZC01 was purified by nickel column chromatography and identified by SDS-PAGE electrophoresis. JZC01 was identified further by Western blot assays that used mouse anti-his antibody and mouse anti-human MICA antibody.

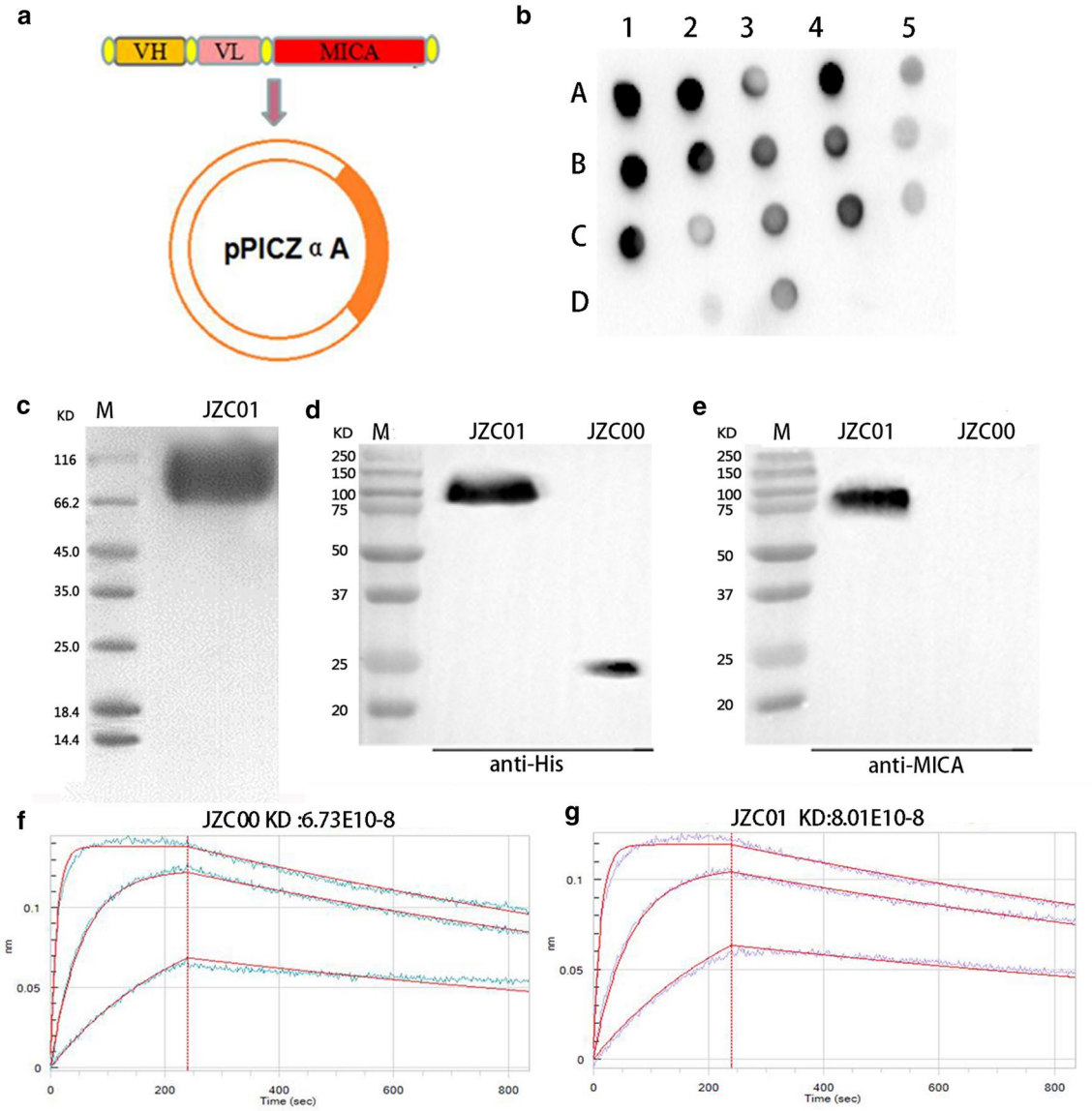

Fig. 1 Design and characterization of bispecific antibody JZC01. **a** Construction of JZC01 expression vector. VH and VL represent cDNA of single chain antibody JZC00; JZC01 sequence was composed of JZC00 and MICA genes in tandem. Then, the gene of JZC01 was integrated into expression vector pPICZαA. **b** High-yielding cloned strain was selected by Dot Blot, positive control, a his tag protein, D2 (0.1 μg/ml), D3 (1 μg/ml), and the negative control D1 (medium). **c** Non-reducing SDS-PAGE analysis of the purified JZC01, M: marker. Purified JZC01 was subjected to Western blot analysis using anti-his tag antibody (**d**) or anti-human MICA antibody (**e**). Binding sensorgrams of the captured JZC00 (**f**) and JZC01 (**g**) interacted with human VEGFR2 and 1:1 Kinetic Model Fit Overlays in OCTECT RED96. The rough lines represent binding response signals at different human VEGFR2 concentrations, and the overlaid smooth lines represent the fitted curves. The equilibrium dissociation constant (KD) is as follows, between JZC00 and human VEGFR2 (6.73E10-8), between JZC01 and human VEGFR2 (8.01 E10-8)

Affinity measurement

The affinity measurement experiment was performed on a ForteBio OCTECT RED96 instrument using HISIK sensors (PALL 18-0038). JZC00/JZC01 was loaded into a 96-well, tilted-bottom microplate at 3 μg/ml by capturing the his tag. Diluted solutions of human VEGFR2, mouse VEGFR2, and human NKG2D were loaded into another 96-well microplate at 200 μl per well. The affinity of JZC00 to human VEGFR2, and the affinity of JZC01 to human VEGFR2, mouse VEGFR2, and human NKG2D was measured. All samples and assays were prepared in an assay buffer of PBS that included 0.1% BSA. ForteBio's data analysis software was used to fit the data to a 1:1 binding model to extract an association rate and dissociation rate. The KD was calculated using the ratio kd/ka.

Binding activity of JZC01

To evaluate the binding activity of JZC01 to VEGFR2-overexpressing cells and NKG2D-expressing cells, LLC, MFC, and NK92 cells were collected and suspended in PBS that included 2% fetal bovine serum. Then, 5×10^5 cells per sample were incubated with 200 nM JZC00 or JZC01 or rMICA or DC101 at 4 °C for 1 h, and the control groups were blocked with 5% skim milk. After incubation, samples were washed three times, stained with PE-conjugated anti-his tag antibody (Biolegend, USA) in the dark for 30 min, and analyzed by flow cytometry (NovoCyte, ACEABIO, USA). The positive control DC101 was stained with PE-conjugated goat anti-rat IgG antibody (Biolegend, USA). The immunofluorescence experiment was performed to assess the binding ability of JZC01 to LLC cells. Briefly, cells were fixed in 2% paraformaldehyde for 20 min and then incubated with JZC00 or JZC01 (200 nM each antibody in 1% BSA-PBS buffer) for 1 h. After being washed three times, cell samples were stained with fluorescein isothiocyanate (FITC)-conjugated anti-his antibody and further imaged by a confocal microscope.

Cell proliferation assay

The proliferation of tumor cells was tested by an MTT assay (Thermo). LLC and MFC cells (5×10^3 cells/well) were plated into a 96-well plate and incubated at 37 °C for 24 h before treatment with a serially diluted JZC01 or JZC00 or DC101 that ranged from 0 to 500 nM. After 72 h, the proliferation was determined using MTT reagent, and the calculation of anti-proliferative activity was as follows: inhibition % = [1 − (experimental-blank)/(control-blank)] × 100%.

Measurement of apoptosis

LLC and MFC cells were plated into a six-well plate at 4×10^5/well and incubated with JZC00 (200 nM), JZC01 (200 nM), or DC101 (100 nM) at 37 °C for 48 h. Then, cells were collected for an Annexin V-FITC/PI apoptosis assay (Sangon Biotech, Shanghai, China) and Bcl-2 family protein (Cell Signaling, USA) detection. Apoptosis of tumor cells was determined by flow cytometry and analyzed further using NovoExpress software. Protein preparation, quantification, and Western blot analyses were performed to further verify the apoptosis pathway-related proteins of Bak, Bax, Bcl-2, and Bcl-XL.

Murine NKG2D expression and cytotoxicity assay

For analysis of NKG2D expression on mouse NK and $CD8^+$ T cells, splenic lymphocytes were extracted and stained with CD49b, CD8a, and NKG2D antibodies (Biolegend, USA). To test the cytotoxicity of JZC01 to tumor cells, quantitative levels of murine spleen lymphocytes were collected and cultured in RPMI 1640 medium that contained 2000 U/ml IL-2 (Sino Biological, Beijing, China) for 4 d. After stimulation with IL-2, the lymphokine-activated killer (LAK) cells were collected, the NKG2D expression on LAK cells was determined, and the activated lymphocytes were used as effector cells for a cytotoxicity assay. The target cells were co-cultured with various amounts of splenic lymphocytes for 4 h at 37 °C in the presence of JZC01. Then, 120 µl of supernatant from each well was analyzed using a lactate dehydrogenase (LDH) cytotoxicity assay kit (Beyotime, China).

Engagement of human NKG2D by JZC01

To verify further that JZC01 engaged NKG2D and activated NKG2D receptors on human $CD8^+$ T and NK cells, we used EasySep™ (STEMCELL Technologies) to isolate human $CD8^+$ T cells and human NK cells from PBMCs; PBMC was harvested from human volunteers by density gradient centrifugation using Ficoll (Sigma-Aldrich). Then, $CD8^+$ T cells were stimulated with anti-CD3 Dynabeads™ and 1 µg/ml human CD80-hFc because pre-activated $CD8^+$ T cells improve the expression of NKG2D [8]. NKG2D expression on $CD8^+$ T and NK cells was measured by flow cytometry. We performed an NK cytotoxicity experiment, which was similar to LAK cytotoxicity. On the other hand, JZC01 or JZC00 or rMICA was coated on the 96-well plate (0.1 µg/ml, 1 µg/ml, 10 µg/ml for each separately). Cytokine-stimulated NK cells or activated $CD8^+$ T cells were plated at 10^5 cells per well in the above protein-coated plate. IFN-γ secretion in the supernatant was determined after 72 h following the instructions of the human IFN-gamma DuoSet kit (DY285B, R&D). The rNKG2D was used for the blocking of JZC01 that interacted with NKG2D-expressing lymphocytes in the experiments mentioned above.

Anti-tumor efficacy of JZC01 in vivo

An LLC xenograft model was established by subcutaneous injection of LLC cells (5×10^6) into the right flanks of 6-week-old c57BL/6 mice. When the average tumor volume reached 100 mm^3, the tumor-bearing mice were divided randomly into seven groups and treated with JZC01 (0.5 mg/

kg, 1 mg/kg, 2 mg/kg) or JZC00 (2 mg/kg) or docetaxel (10 mg/kg) or a combination of JZC01 and docetaxel (2 mg/kg + 10 mg/kg) or saline by intravenous injection. The progression of tumors in LLC tumor-bearing mice was measured every other day, and the tumor volume was calculated with the formula $V = L \times W^2/2$ (L: longest diameter of tumor, W: maximum transverse diameter of vertical direction).

Tumor-infiltrating lymphocyte analysis

The LLC tumor-bearing mice were treated with JZC01 (2 mg/kg) or saline intravenously on day 0, 2, 4, 6, and 8. On day 10, mice were killed. Tumor tissues were collected and ground into single suspension cells. A mononuclear cell-enriched fraction was isolated using Percoll centrifugation media (Tbdscience, Tianjin, China). TIL was analyzed by staining with CD3, CD8a, CD49b, NKG2D, CD69, and CD107a (FcMRCS, Nanjing, China), and the proportion of $CD8^+$ T cells and activated NK cells in the tumor tissues was detected by flow cytometry.

Immunohistochemistry, HE staining, and immunofluorescence analysis

Paraffin sections of tumor tissues were cut into 5 μm sections. For immunohistochemical (IHC) staining, samples were incubated with antibodies against Ki67, CD31, and VEGF (Cell Signaling Technology, USA). For the immunofluorescence assay, sections were incubated with fluorescent-labeled antibodies against IFN-γ and TNF-α (Abcam, Cambridge, UK) and then stained with DAPI (SunBio Technology, Nanjing, China). The pulmonary metastasis of tumor-bearing mice was evaluated by HE staining of the lung tissues. All of the slides were imaged under a fluorescence microscope.

Results

Generation and identification of JZC01

JZC01 was a novel bispecific antibody, which was generated by fusing the single chain antibody (JZC00) and the extracellular domains of human MICA. The yeast vector pPICZαA was integrated with the fusion gene of JZC01 (Fig. 1a), transformed into Pichia X-33, and a high-yielding cloned strain was selected by Dot blot (Fig. 1b). JZC01 was purified by nickel affinity chromatography, and the purified JZC01 was homogenous with the expected molecular weight by SDS-PAGE electrophoresis (Fig. 1c). JZC01 was validated by Western blot analysis that utilized mouse anti-his antibody (Fig. 1d) and mouse anti-human MICA antibody (Fig. 1e). The affinity of JZC00 and JZC01 to human VEGFR2 was measured using ForteBio OCTECT RED96, and the binding profiles of JZC00 (KD 6.73E−8) and JZC01 (KD 8.01E−8) were similar across the ForteBio (Fig. 1f, g). Because JZC01 cross-reacted with mouse VEGFR2, the affinity of JZC01 to mouse VEGFR2 was detected in the same condition as to human VEGFR2, and the KD value was 2.39E10−7 (Fig. 2a). The affinity of JZC01 to human NKG2D was 8.89E10−7 (Fig. 2b), which was similar to the reported affinity data of MICA to NKG2D [35].

JZC01 bound to VEGFR2 and NKG2D

JZC01 targeted human VEGFR2, but recognized mouse VEGFR2. To identify the binding capacity of JZC01 to murine cancer cell lines MFC and LLC, flow cytometry and a confocal microscope were used. According to the results of flow cytometry, JZC01 showed considerable binding capacity to LLC cells and MFC cells. Moreover, JZC01 and JZC00 possessed similar binding to those two cell lines, but little binding was seen with rMICA treatment (Fig. 2c, d) and DC101was set as a positive control. JZC01 and JZC00 bound to LLC cells on the graph of the confocal diagram, which indicated abundant VEGFR2 expression on the LLC cell membranes (Fig. 2f–h). In addition, we also demonstrated the binding capacity of JZC01 to NKG2D-expressing cells NK92. JZC01 and the recombinant MICA exhibited good binding capacity to NK92 cells, but not JZC00 (Fig. 2e).

JZC01 inhibited proliferation and promoted apoptosis of tumor cells

To determine the cytotoxicity of JZC01 on murine LLC and MFC cells, cells were exposed to different concentrations of JZC01 that ranged from 0 to 500 nM for 72 h. MTT analysis showed that JZC01 treatment resulted in inhibition of the growth of LLC cells (Fig. 3a) and MFC cells (Fig. 3b), and the inhibition was dose dependent. To investigate whether the inhibition was related to VEGFR2-mediated cell apoptosis, LLC cells were treated with JZC01 or JZC00 or DC101 for 48 h, stained with AnnexinV-FITC/PI, and analyzed by flow cytometry. At the same dose level of 200 nM, the apoptosis rate of JZC00 (Fig. 3c) and JZC01 (Fig. 3d) was roughly similar. DC101 was set as the positive control (Fig. 3e), and PBS was set as the negative control (Fig. 3f). Quantitative analysis of the apoptosis rate (sum of Q2–2 and Q2–4) was performed for three parallel experiments (Fig. 3g). To determine the signaling pathway related to apoptosis, Western blot was used to examine the expression of Bcl-2, Bax, Bak, and Bcl-Xl. JZC01 treatment resulted in decreased expression of Bcl-2 and Bcl-Xl,

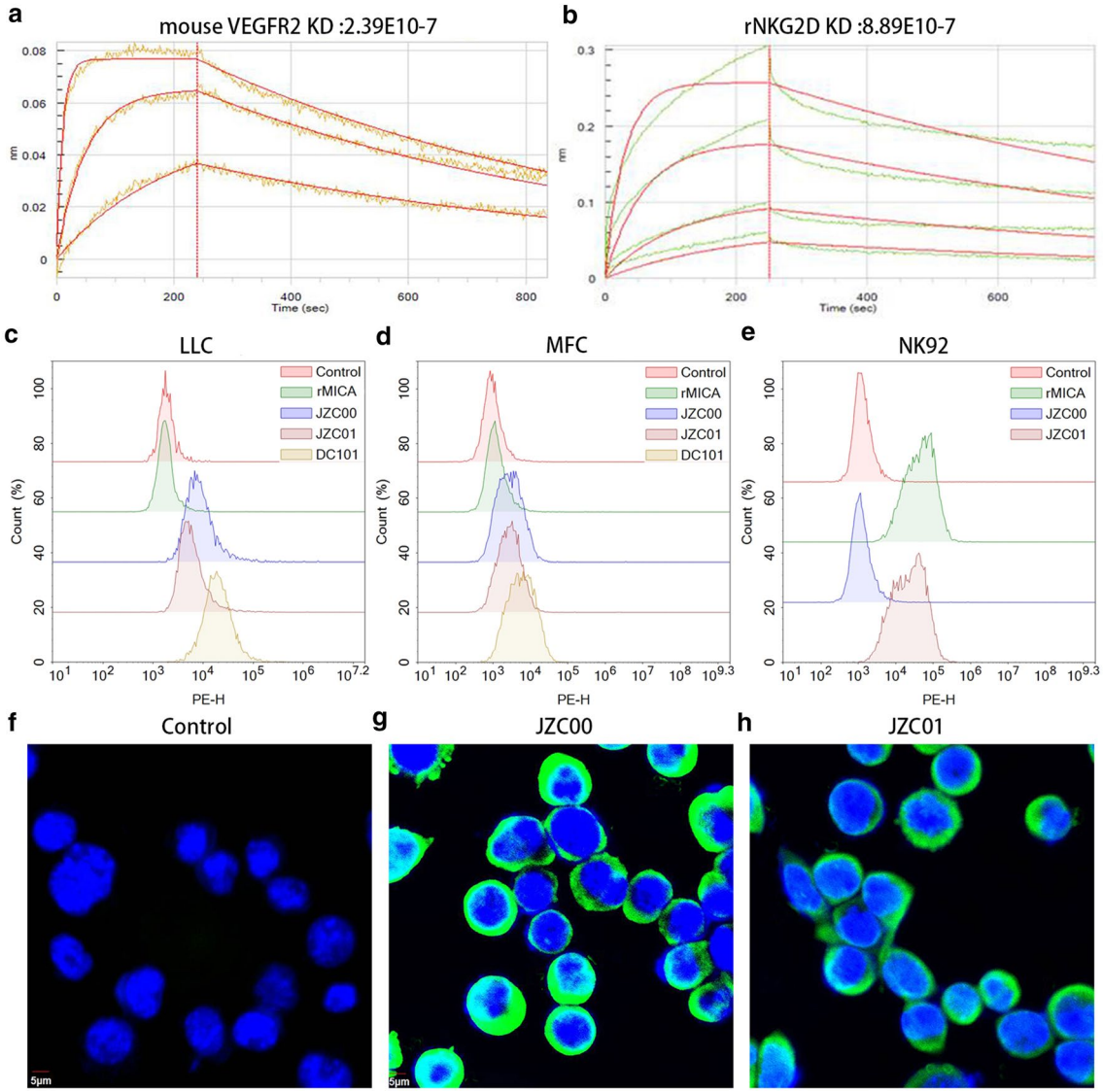

Fig. 2 JZC01 bound specifically to mouse VEGFR2 and human NKG2D. Binding sensorgrams of the captured JZC01 interacted with mouse VEGFR2 and rNKG2D. **a** JZC01 bound specially to mouse VEGFR2 with the affinity 2.39E10-7. **b** JZC01 bound to rNKG2D with the affinity 8.89E10-7. JZC01, JZC00, and DC101 bound to mouse cancer cell lines, LLC (**c**) and MFC (**d**). **e** JZC01 and rMICA bound to NKG2D-positive NK92 cells but not to JZC00. **f**–**h** Immunofluorescence was used to visually illustrate the binding activity of JZC00 (**g**) and JZC01 (**h**) to mouse tumor cell line LLC. DC101 was a commercial anti-mouse VEGFR2 antibody

but increased expression of Bax and Bak (Fig. 3h). Similar results were found for MFC cells with the same treatment (data not shown).

JZC01-mediated cytotoxicity to VEGFR2-expressing tumor cells

A commercial antibody specific for mouse NKG2D was used to examine the cell surface expression of NKG2D on mouse NK and $CD8^+$ T cells. Nearly all $CD49b^+$ splenocyte cells from adult c57BL/6 expressed NKG2D ($n = 5$, Supplementary Fig. 1a) and relatively smaller percentages of $CD8^+$ T cells present in the NKG2D-positive area ($n = 5$, Supplementary Fig. 1b). To investigate NKG2D-mediated cytotoxicity, NKG2D-expressing LAK cells were obtained by stimulation and confirmed by flow cytometry. A total of 16.1% of LAK cells were NKG2D positive (Supplementary Fig. 1c). We performed a cytotoxicity assay using MFC or LLC as the target cells and LAK as the effector cells. We measured cytotoxicity using serial concentrations of JZC01 (from 0.001 to 1000 μg/mL) at a fixed effector cell to target cell (E:T) ratio of 100:1. We found that JZC01 triggered stronger cellular cytotoxicity

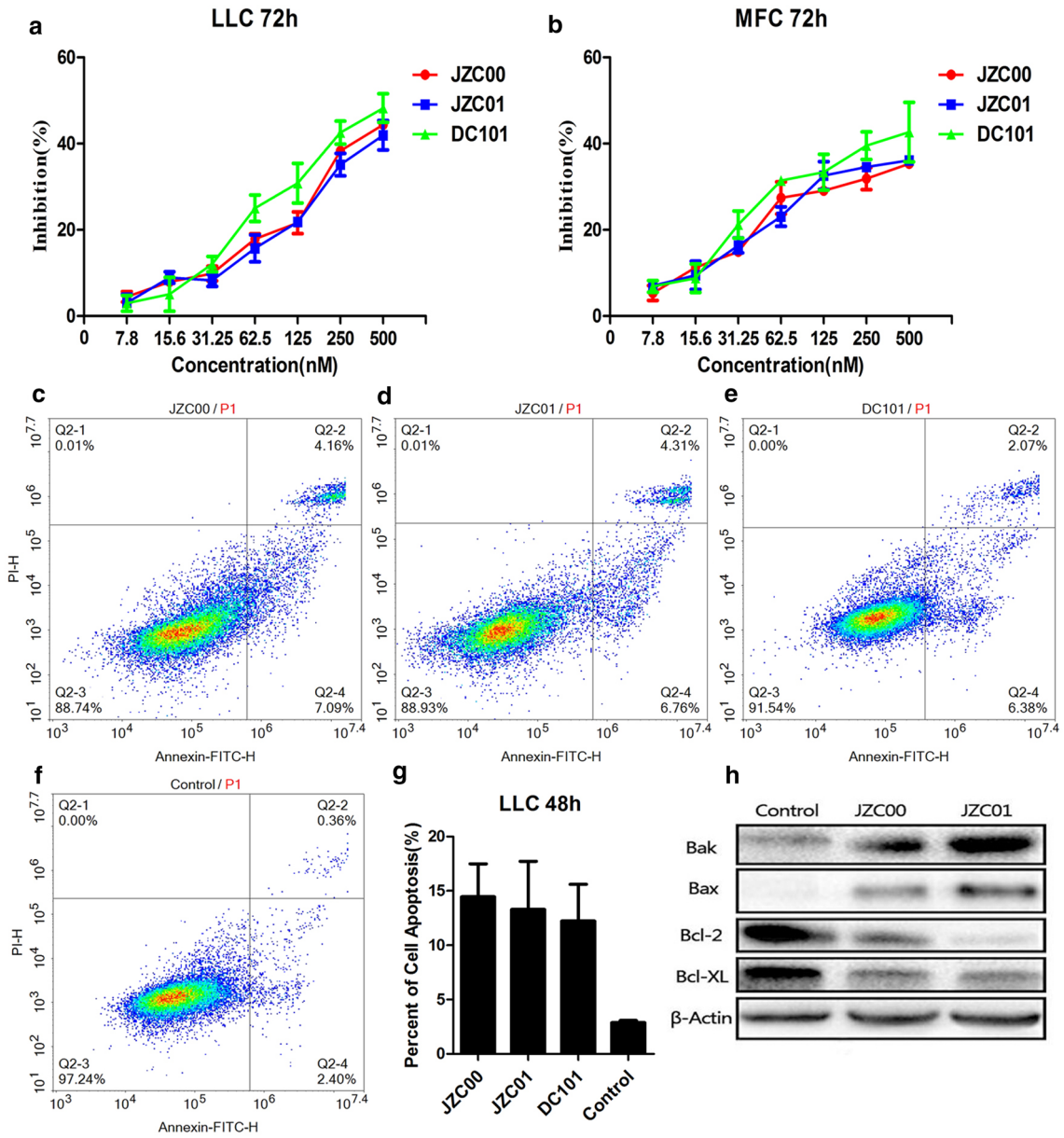

Fig. 3 JZC01 inhibited proliferation and induced apoptosis of LLC and MFC cells. **a**, **b** MTT assay showed that JZC01 inhibited the proliferation of LLC and MFC cells, similar to JZC00. Bivalent antibody DC101was set as the positive control. LLC cells were incubated with 200 nM JZC00 (**c**) or 200 nM JZC01 (**d**) or 200 nM DC101 (**e**) or PBS (**f**) at 37 °C for 48 h, after staining with Annexin V-FITC and PI and analyzed by flow cytometry. The percentage of apoptotic cells in each quadrant is indicated. **g** Quantitative analysis of apoptosis rate (data were presented as the mean ± SD, $n = 3$). **h** Western blot analysis for Bcl-2, Bax, Bak, and Bcl-Xl of LLC cells treated with JZC01 or JZC00. Equal loading of protein was confirmed by stripping the immunoblot and reprobing it for β-actin

(Supplementary Fig. 1d, e) and the cell lysis was dose dependent. LAK cells were co-cultured with LLC or MFC cells in the presence of an optimal concentration of JZC01. Enhanced cell lysis was seen with the JZC01 treatment following an increase in the E:T ratio. The lysis rate remained almost unchanged in the JZC00 and rMICA groups (Fig. 4a, b), which indicated that JZC01 bridged LAK cells and targeted cells to mediate cell lysis.

JZC01 engaged human NKG2D and mediated cell lysis and cytokine release

Human NK and $CD8^+$ T cells expressed NKG2D constitutively, although NKG2D is considered to be a co-stimulatory signal for $CD8^+$ T cell activation. To promote activation, NK and $CD8^+$ T cells were separated and cultured for 2 days with stimulators introduced in the method and detected for NKG2D expression (Fig. 4c, d).

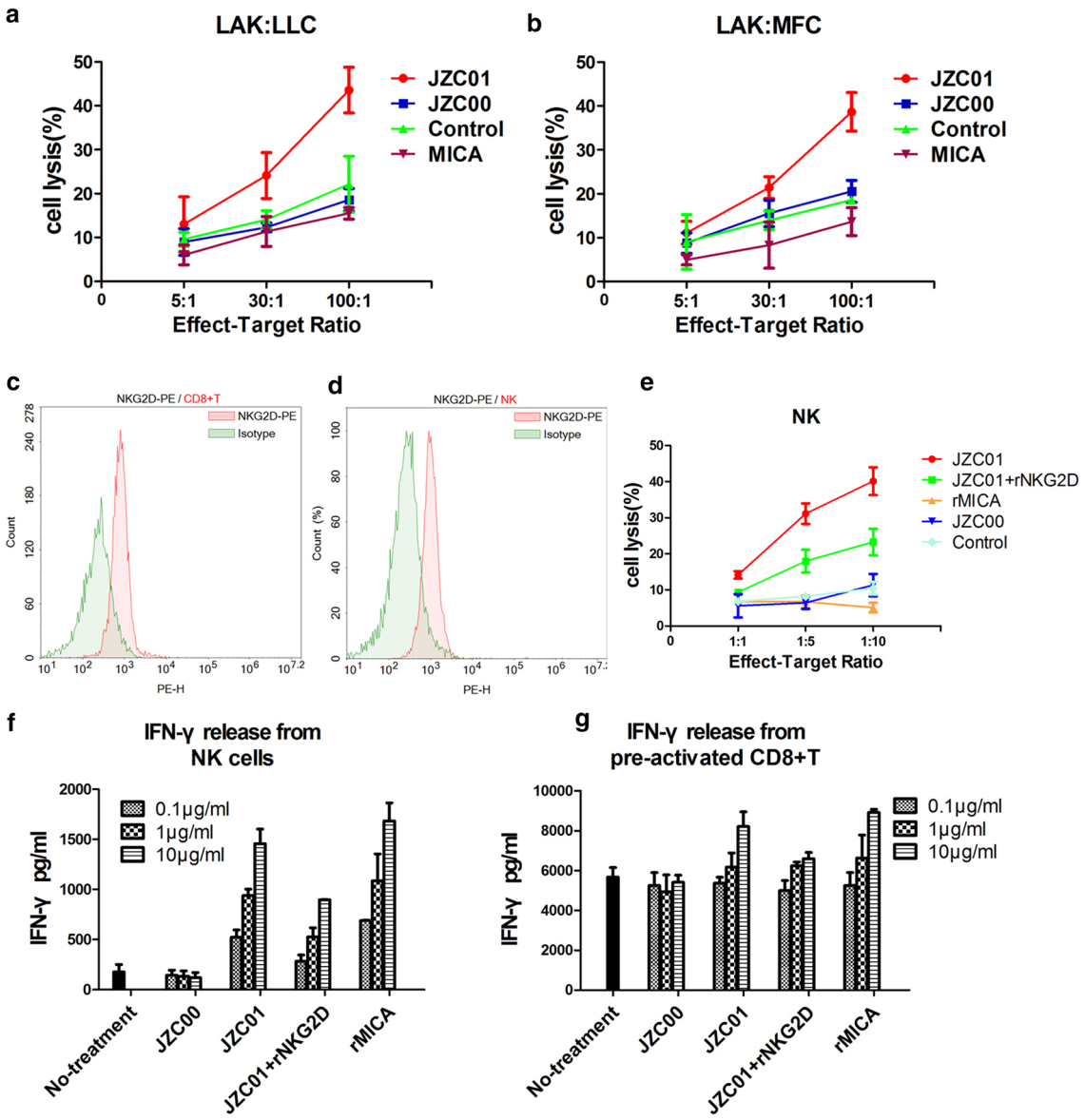

Fig. 4 NKG2D-expressing cells mediated cytotoxicity and increased IFN-γ release. High concentration of IL-2-activated mouse spleen cells (LAK cells) were incubated with LLC (**a**) or MFC (**b**) cells in the presence of JZC01. The E:T ratios are indicated. The NKG2D expression on activated $CD8^+$ T (**c**) and NK (**d**) cells was measured by flow cytometry. **e** JZC01 (10 μg/ml) engaged human NK cells to lysis LLC cells, which was inhibited by rNKG2D. **f** IFN-γ release in the supernatant of IL-2- and IL-15-activated NK cells increased when presented with JZC01 or rMICA, but they were impaired with rNKG2D. **g** IFN-γ release in the supernatant of activated $CD8^+$ T cells increased when presented with JZC01 or rMICA, but they were impaired with rNKG2D

NK cells were co-cultured with LLC cells in the presence of 10 μg/ml JZC01, and cell lysis was observed in the JZC01 treatment. The lysis rate decreased with 10 μg/ml rNKG2D (Fig. 4e), which suggested that JZC01 engaged human NK cells through NKG2D to exert cytotoxicity. The immobilized JZC01 and rMICA promoted the release of IFN-γ in the presence of NK (Fig. 4f) or $CD8^+$ T (Fig. 4g) cells, but the release of IFN-γ decreased when rNKG2D was added. Taken together, JZC01 targeted VEGFR2-expressing tumor cells and engaged NKG2D receptors on NK and $CD8^+$ T cells, which induced NKG2D-mediated activation.

JZC01 enhanced anti-tumor efficacy in tumor-bearing mice

LLC cells were inoculated to the armpit of c57BL/6 mice subcutaneously, and tumor volumes were measured during the treatment (Fig. 5a). At the end of the treatment, the growth of tumors was significantly inhibited in

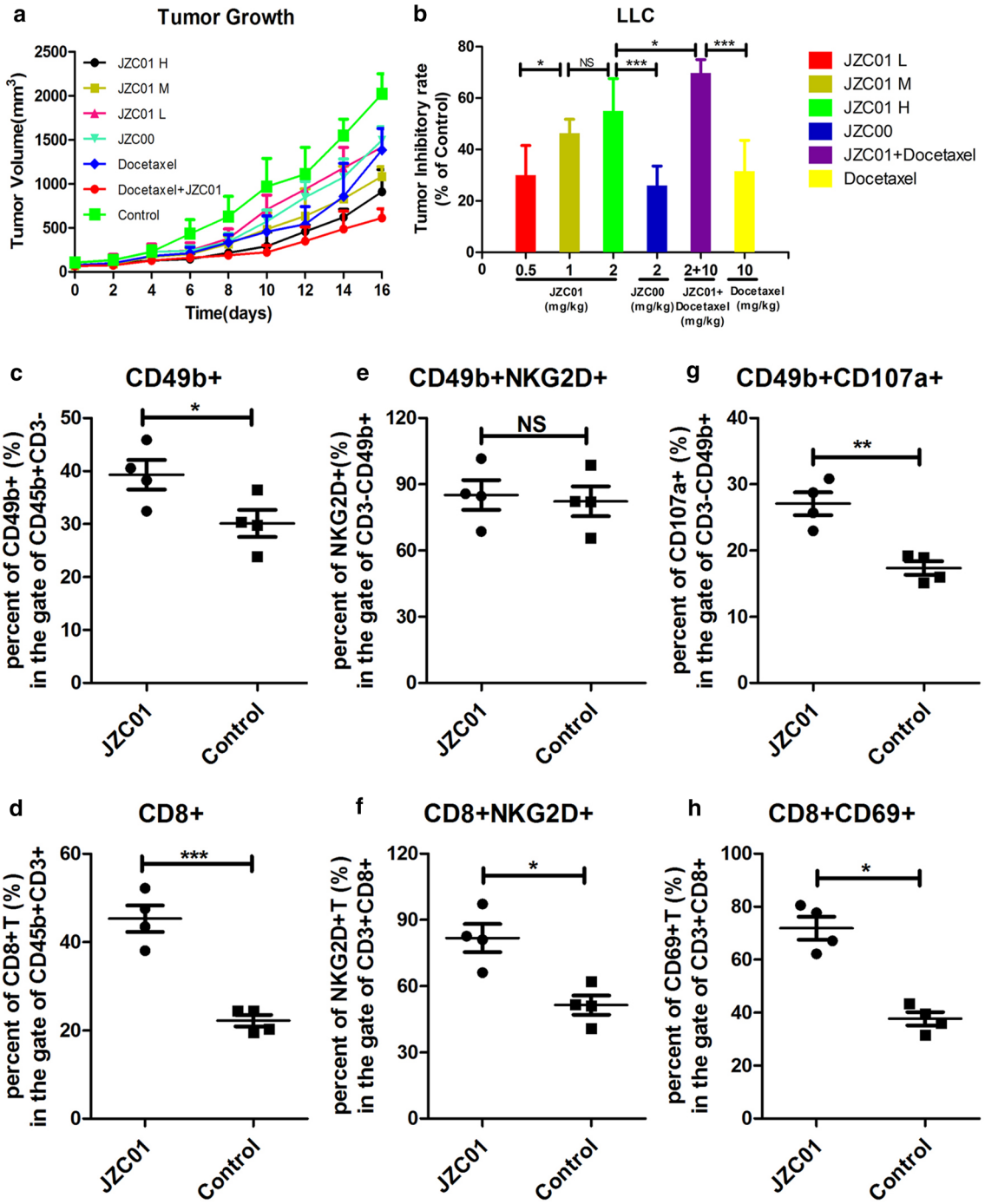

Fig. 5 JZC01 demonstrated efficacy against an LLC tumor xenograft and recruited NK/CD8$^+$T cells in an LLC tumor microenvironment. **a** Tumor growth curves for c57BL/6 mice. Mice were divided into six groups for different treatments, and the tumor volume was measured following tumor development. **b** Tumor inhibition rates of different dosage groups. JZC01 significantly improved the tumor inhibition rate compared with JZC00. **c**, **e**, **g** The relative percentages of live intratumor CD49b$^+$, CD49b$^+$NKG2D$^+$, and CD49b$^+$CD107a$^+$ lymphocytes from tumors ($n=4$) of JZC01 and saline treatment groups. **d**, **f**, **h** The relative percentages of live intratumor CD8a$^+$, CD8a$^+$NKG2D$^+$, and CD8a$^+$CD69$^+$ lymphocytes from tumors ($n=4$) of JZC01 and saline treatment groups. All data were presented as the mean ± SD, $^*p<0.05$, $^{**}p<0.01$, $^{***}p<0.001$

JZC01-treated groups, and the tumor burden was reduced by 55.4% (high dose). Moreover, JZC01-treated LLC-bearing mice showed stronger inhibition of tumor growth than the JZC00 group (Fig. 5b), which demonstrated that antibody fusion with MICA enhanced the anti-tumor effect in vivo. To investigate further the potential clinical utility of JZC01 in

the treatment of cancer, we decided to test the combination therapy of JZC01 with the chemotherapeutic drug docetaxel. Docetaxel is a chemotherapy medication and is used to treat a number of solid cancers and to suppress microtubule dynamic assembly and disassembly. The combination of ramucirumab and docetaxel has been approved for NSCLC treatment. In this study, docetaxel combined with JZC01 reduced tumor volume further and verified the potential use of JZC01 combined with chemotherapeutic agents.

JZC01 improved lymphocyte infiltration and activation in tumor areas

Tumor-bearing mice were treated with JZC01 for 10 days, and TILs were extracted from the tumor tissues. The status of infiltration and activation of intratumor $CD8^+$ T cells and NK cells was measured by flow cytometry. A greater number of $CD8^+$ T cells (Fig. 5c) and NK cells (Fig. 5d) were seen in the tumor microenvironment in the JZC01-treated group. Next, the expression of NKG2D and the activated markers CD69 and CD107a were quantified. Compared with the control group, NKG2D expression in JZC01-treated intratumoral $CD8^+$ T cells was up-regulated (Fig. 5f), but on intratumoral NK cells, the NKG2D expression was unchanged (Fig. 5e). CD69 was expressed on the early activated T cells and was involved in differentiation and proliferation of T cells. CD107a is a sensitive marker of degranulation for activated NK cells. In this model, after administration for 10 days, a higher percentage of $CD8^+CD69^+$ T cells and $CD49b^+CD107a^+$ NK cells was observed in the JZC01 group (Fig. 5g, h), which indicated that JZC01 induced the activation of NK and $CD8^+$ T cells in the tumor. In addition, more TNF-α (Fig. 6g, h) and IFN-γ (Fig. 6i, j) was detected in the tumor tissues of JZC01 treatment by immunofluorescent assay, which suggested that JZC01 increased cytokine release and activated the tumor microenvironment. Altogether, these results indicated that there was recruitment and activation of NK and $CD8^+$ T cells in the JZC01-treated tumor microenvironment.

JZC01 inhibited proliferation, angiogenesis, and pulmonary metastasis in tumor xenografts

To investigate further the anti-tumor effect of JZC01, we studied tumor growth under different treatments using an immunohistochemistry assay. Compared with the control group, there was a significant decrease in the intensity of cell proliferation marker Ki67 in the JZC01-treated group and a slight decrease in the JZC00-treated group (Fig. 6a, b). Less expression of CD31 (Fig. 6c, d) and VEGF (Fig. 6e, f) was observed in the JZC01 treatment, which demonstrated that JZC01 down-regulated angiogenesis in tumor tissues compared with the control and the JZC00 group. This was probably because activation of tumor immunity inhibited tumor growth and reduced angiogenesis. In addition, severe pulmonary metastasis was observed in tumor-bearing mice of the control group ($n = 5$, Supplementary Fig, 2a). An obvious tendency for pulmonary metastasis ($n = 5$, Supplementary Fig. 2b) occurred in the JZC00-treated group, although it was restrained completely in the JZC01 treatment ($n = 5$, Supplementary Fig. 2c). Thus, the results of IHC and HE staining demonstrated that JZC01 treatment played a remarkable role in inhibiting angiogenesis and metastasis.

Statistical analysis

Data were expressed as the mean ± SD. Mann–Whitney *U* test was used to evaluate significance levels between two groups, and a *p* value of 0.05 or less was considered statistically significant. GraphPad Prism software (San Diego, CA) was used for data processing.

Discussion

Anti-angiogenesis with VEGF blocking agents is the most conventional approach to control tumor angiogenesis. A combination of anti-angiogenesis and anti-tumor immune activation shows promise for treating solid tumors [36–38]. Our design of the bispecific antibody JZC01, which enabled anti-angiogenesis and activation of anti-tumor immunity, was novel. In vitro study, blocking the VEGFR2 signal pathway, restricted cell proliferation and induced cell apoptosis. Also, JZC01 induced a strong activation of NK and a co-activation of $CD8^+$ T cells by increasing the secretion of IFN-γ and mediated cytotoxicity to target cells. By targeting VEGFR2, JZC01 decreased tumor vascular density in a tumor-bearing mouse model. Moreover, in the animal study, JZC01 promoted a tumor-inflammatory response with increased infiltration of NK and $CD8^+$ T cells and production of IFN-γ and TNF-α, which resulted in inhibition of tumor growth.

MICA shedding from tumors often results in insensitivity to NK killing. The idea of a single chain antibody fusion with MICA to enhance the NK immune surveillance was verified. A CD24 single chain antibody fusion with MICA increased anti-tumor activity significantly in an HCC-bearing nude mice model by enhancing NKG2D-mediated immune surveillance [34]. However, the role of JZC01 in immune regulation of NKG2D-expressing $CD8^+$ T cells is unknown. It has been reported that MICA-NKG2D activation is a co-stimulatory activation signal for $CD8^+$ T cells [8]. Here, we observed that in the presence of an activation signal for CD3 and CD28, NKG2D activation by JZC01 enhanced the release of IFN-γ in $CD8^+$ T cells. In this study, we observed effective recruitment and activation of NK cells

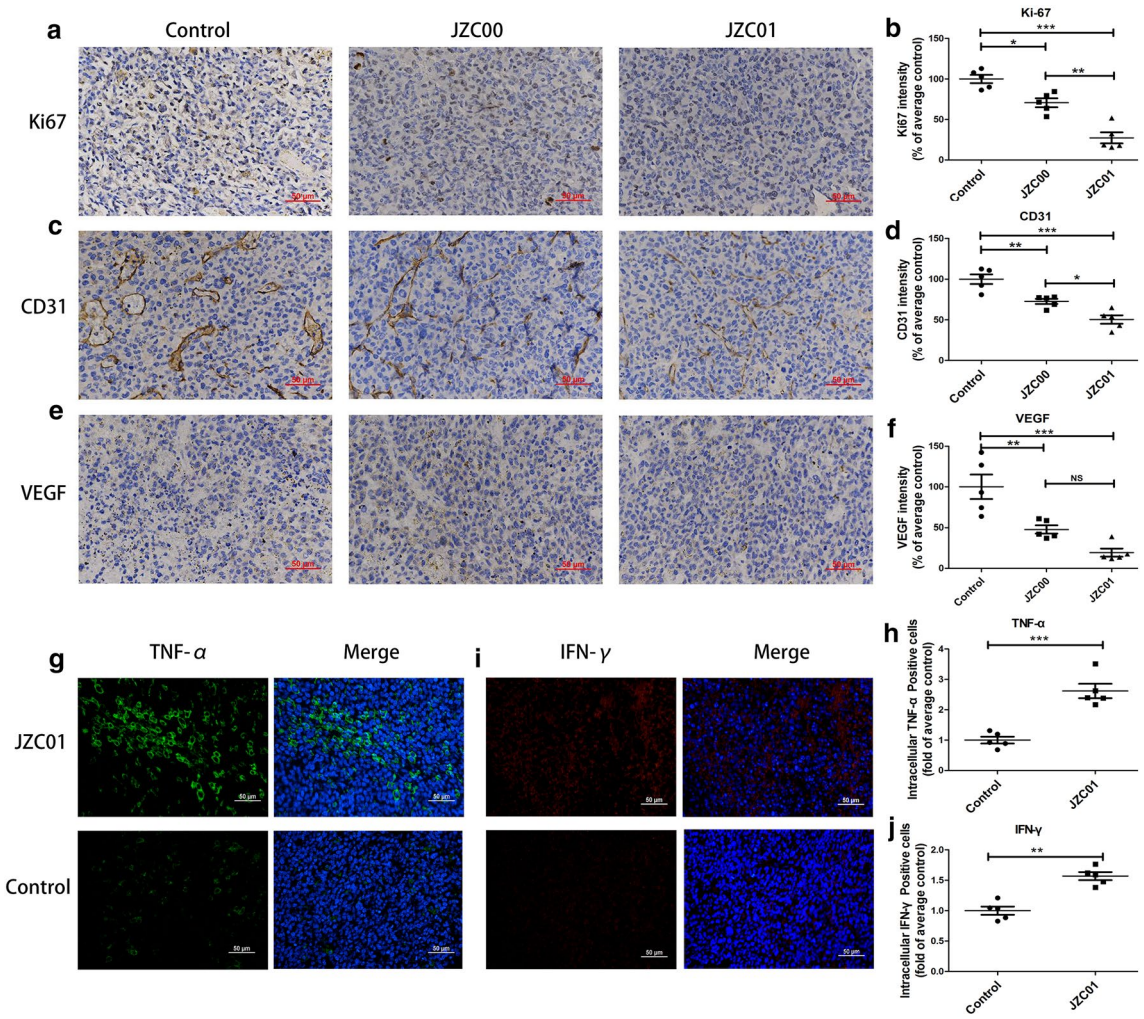

Fig. 6 JZC01 reduced markers of proliferation and angiogenesis and increased the production of IFN-γ and TNF-α in the tumor microenvironment. IHC staining of Ki-67 on paraffin sections of tumor tissues. **a** Ki-67$^+$ cells were identified with an anti-Ki-67 antibody (brown staining). **c** IHC staining of CD31. The CD31$^+$ blood vessels were identified with an anti-CD31 antibody (brown staining). **e** IHC staining of VEGF was identified by VEGF staining. Immunofluorescence double staining of TNF-α (green fluorescence) and IFN-γ (red fluorescence) to determine the expression level of TNF-α (**g**) and IFN-γ (**i**) in the tumor tissue. Densitometric analysis was performed by Image J to quantify Ki-67 (**b**), CD31 (**c**), VEGF (**f**), TNF-α (**h**), and IFN-γ (**j**). All data were presented as the mean ± SD, $n = 5$, $^*p < 0.05$, $^{**}p < 0.01$, $^{***}p < 0.001$

and CD8$^+$ T cells in a mouse model. Ligands of NKG2D may induce down-modulation of NKG2D receptor [20], but, in our study the MICA fusion antibody JZC01 increased NKG2D-positive CD8$^+$ T cells in the tumor-infiltrating lymphocytes. This may have been due to the enhanced tumor recognition by NK killing and promotion of tumor antigens presentation, which increased the production and activation of tumor-specific T cells [39].

In the LLC tumor-bearing model, presenting more MICA to the tumor microenvironment by targeting VEGFR2 was an effective anti-tumor strategy; this caused more NK and CD8$^+$ T cells to infiltrate the tumor, which released more IFN-γ/TNF-α in the treatment using JZC01. In addition to the anti-tumor effect by immune activation, JZC01 inhibited tumor angiogenesis, which is characterized as an essential process for proliferation and viability of tumor cells. Immunohistochemistry showed that both the microvessel density and the release of VEGF apparently decreased in tumor tissue in the JZC01 treatment group compared with the control group and the JZC00 group. JZC01 activated NKG2D receptors and enhanced IFN-γ production in vitro and in vivo. However, IFN-γ directly down-regulates the expression of delta-like protein 4 on endothelial cells [40] and the secretion of VEGF by tumor-associated fibroblasts [41], which are critical for sprouting angiogenesis. Therefore, immune activation may have induced changes in the tumor vasculature and generated a more potent anti-angiogenesis [42].

In summary, this study showed that the novel bispecific antibody JZC01 was capable of anti-tumor immune activation and anti-angiogenesis in a tumor-bearing mouse model. More importantly, JZC01 activated the tumor microenvironment by enhancing NKG2D activation, which could be developed further as immunotherapy for more malignancies. Also, the combination therapy of JZC01and docetaxel provided new insights into enhancing efficacy and outlined potential applications of JZC01.

Author contributions YX and XZ designed and performed the experiments. YW guided the affinity measurement and cell-based binding assay. MP helped with the NK and $CD8^+$ T cells isolation and IFN-γ detection. JZ, MW, and YW designed the study. YX and JZ wrote the paper.

Funding This work was supported in part by the National Natural Science Foundation of China (NSFC 81973223), Natural Science Foundation of Jiangsu Province (BK20161459), Jiangsu Province Qinglan Project (2014); "Double First-Class" University project (CPU2018PZQ12 and CPU2018GY14).

Compliance with ethical standards

Conflict of interest The authors declare that they have no conflict of interest.

Ethical approval and ethical standards This article does not contain any studies with human participants performed by any of the authors. This study was approved by the Ethics Review Committee of China Pharmaceutical University (9 March 2016). All applicable international, national, and/or institutional guidelines for the care and use of animals were followed. Six-week-old c57BL/6 healthy female mice were purchased from Comparative Medicine Centre of Yangzhou University (Yangzhou, China). All animals were housed in a pathogen-free environment and were treated following the standards of Pharmaceutical Animal Center of China Pharmaceutical University (Approval number XYXK-2016-0011).

Cell line authentication Murine cancer cell lines, Lewis lung carcinoma (LLC) (CRL-1642, ATCC), and mouse forestomach gastric carcinoma (MFC) (100207, BNCC) were obtained from Shanghai cell bank, Chinese Academy of Sciences. No cell line authentication was necessary since the phenotypes of these cells were checked by Shanghai cell bank before we obtained them and they did not change over time.

References

1. Sharma P, Hu-Lieskovan S, Wargo JA, Ribas A (2017) Primary, adaptive, and acquired resistance to cancer immunotherapy. Cell 168(4):707–723. https://doi.org/10.1016/j.cell.2017.01.017
2. Waldhauer I, Goehlsdorf D, Gieseke F, Weinschenk T, Wittenbrink M, Ludwig A, Stevanovic S, Rammensee HG, Steinle A (2008) Tumor-associated MICA is shed by ADAM proteases. Can Res 68(15):6368–6376
3. Raulet DH, Gasser S, Gowen BG, Deng W, Jung H (2013) Regulation of ligands for the NKG2D activating receptor. Annu Rev Immunol 31:413–441. https://doi.org/10.1146/annurev-immunol-032712-095951
4. Gasser S, Orsulic S, Brown EJ, Raulet DH (2005) The DNA damage pathway regulates innate immune system ligands of the NKG2D receptor. Nature 436(7054):1186–1190. https://doi.org/10.1038/nature03884
5. Spear P, Wu MR, Sentman ML, Sentman CL (2013) NKG2D ligands as therapeutic targets. Cancer Immun 13(2):8
6. Groh V, Rhinehart R, Randolph-Habecker J, Topp MS, Riddell SR, Spies T (2001) Costimulation of CD8 alphabeta T cells by NKG2D via engagement by MIC induced on virus-infected cells. Nat Immunol 2(3):255–260. https://doi.org/10.1038/85321
7. Bauer S, Groh V, Wu J, Steinle A, Phillips JH, Lanier LL, Spies T (1999) Activation of NK cells and T cells by NKG2D, a receptor for stress-inducible MICA. Science 285(5428):727–729
8. Hu J, Batth IS, Xia X, Li S (2016) Regulation of $NKG2D^+CD8^+$ T-cell-mediated antitumor immune surveillance: identification of a novel CD28 activation-mediated, STAT3 phosphorylation-dependent mechanism. Oncoimmunology 5(12):e1252012. https://doi.org/10.1080/2162402X.2016.1252012
9. Kaiser BK, Yim D, Chow IT, Gonzalez S, Dai Z, Mann HH, Strong RK, Groh V, Spies T (2007) Disulphide-isomerase-enabled shedding of tumour-associated NKG2D ligands. Nature 447(7143):482–486. https://doi.org/10.1038/nature05768
10. Boutet P, Aguera-Gonzalez S, Atkinson S, Pennington CJ, Edwards DR, Murphy G, Reyburn HT, Vales-Gomez M (2009) Cutting edge: the metalloproteinase ADAM17/TNF-alpha-converting enzyme regulates proteolytic shedding of the MHC class I-related chain B protein. J Immunol 182(1):49–53
11. Raffaghello L, Prigione I, Airoldi I, Camoriano M, Levreri I, Gambini C, Pende D, Steinle A, Ferrone S, Pistoia V (2004) Downregulation and/or release of NKG2D ligands as immune evasion strategy of human neuroblastoma. Neoplasia 6(5):558–568
12. Jinushi M, Vanneman M, Munshi NC, Tai YT, Prabhala RH, Ritz J, Neuberg D, Anderson KC, Carrasco DR, Dranoff G (2008) MHC class I chain-related protein A antibodies and shedding are associated with the progression of multiple myeloma. Proc Natl Acad Sci USA 105(4):1285–1290. https://doi.org/10.1073/pnas.0711293105
13. Holdenrieder S, Stieber P, Peterfi A, Nagel D, Steinle A, Salih HR (2006) Soluble MICA in malignant diseases. Int J Cancer 118(3):684–687. https://doi.org/10.1002/ijc.21382
14. Huergo-Zapico L, Gonzalez-Rodriguez AP, Contesti J, Gonzalez E, Lopez-Soto A, Fernandez-Guizan A, Acebes-Huerta A, de Los Toyos JR, Lopez-Larrea C, Groh V et al (2012) Expression of ERp5 and GRP78 on the membrane of chronic lymphocytic leukemia cells: association with soluble MICA shedding. Cancer Immunol Immunother 61(8):1201–1210. https://doi.org/10.1007/s00262-011-1195-z
15. Jia HY, Liu JL, Zhou CJ, Kong F, Yuan MZ, Sun WD, Wang J, Liu L, Zhao JJ, Luan Y (2014) High expression of MICA in human kidney cancer tissue and renal cell carcinoma lines. Asian Pac J Cancer Prev 15(4):1715–1717
16. Liu Y, Guo X, Xing M, Zhao K, Luo L, Du J (2018) Prognostic value of serum levels of soluble MICA (sMICA) in patients with prostate cancer. Br J Biomed Sci 75(2):98–100. https://doi.org/10.1080/09674845.2017.1402405
17. Cascone R, Carlucci A, Pierdiluca M, Santini M, Fiorelli A (2017) Prognostic value of soluble major histocompatibility complex class I polypeptide-related sequence A in non-small-cell lung cancer—significance and development. Lung Cancer (Auckl) 8:161–167. https://doi.org/10.2147/LCTT.S105623
18. Xing S, Zhu Y, Sun Y (2017) Serum smica as biomarker in detection of non-small-cell lung carcinoma. Br J Biomed Sci 2017:1–3
19. Wang LP, Niu H, Xia YF et al (2015) Prognostic significance of serum sMICA levels in non-small cell lung cancer. Eur Rev Med Pharmacol Sci 19(12):2226

20. Groh V, Wu J, Yee C, Spies T (2002) Tumour-derived soluble MIC ligands impair expression of NKG2D and T-cell activation. Nature 419(6908):734–738. https://doi.org/10.1038/nature01112
21. Jayson GC, Kerbel R, Ellis LM, Harris AL (2016) Antiangiogenic therapy in oncology: current status and future directions. Lancet 388(10043):518–529. https://doi.org/10.1016/S0140-6736(15)01088-0
22. Maishi N, Hida K (2017) Tumor endothelial cells accelerate tumor metastasis. Cancer Sci 108(10):1921–1926. https://doi.org/10.1111/cas.13336
23. Arnold D, Fuchs CS, Tabernero J, Ohtsu A, Zhu AX, Garon EB, Mackey JR, Paz-Ares L, Baron AD, Okusaka T et al (2017) Meta-analysis of individual patient safety data from six randomized, placebo-controlled trials with the antiangiogenic VEGFR2-binding monoclonal antibody ramucirumab. Ann Oncol 28(12):2932–2942. https://doi.org/10.1093/annonc/mdx514
24. Sitohy B, Nagy JA, Dvorak HF (2012) Anti-VEGF/VEGFR therapy for cancer: reassessing the target. Cancer Res 72(8):1909–1914. https://doi.org/10.1158/0008-5472.CAN-11-3406
25. Weis SM, Cheresh DA (2011) Tumor angiogenesis: molecular pathways and therapeutic targets. Nat Med 17(11):1359–1370. https://doi.org/10.1038/nm.2537
26. Jung K, Heishi T, Khan OF, Kowalski PS, Fukumura D (2017) Ly6Clo monocytes drive immunosuppression and confer resistance to anti-VEGFR2 cancer therapy. J Clin Invest 127(8):3039–3051. https://doi.org/10.1172/JCI93182
27. Rivera LB, Meyronet D, Hervieu V, Frederick MJ, Bergsland E, Bergers G (2015) Intratumoral myeloid cells regulate responsiveness and resistance to antiangiogenic therapy. Cell Rep 11(4):577–591. https://doi.org/10.1016/j.celrep.2015.03.055
28. Shrimali RK et al (2010) Antiangiogenic agents can increase lymphocyte infiltration into tumor and enhance the effectiveness of adoptive immunotherapy of cancer. Cancer Res 70:6171–6180
29. Huang Y, Yuan J, Righi E, Kamoun WS, Ancukiewicz M, Nezivar J, Santosuosso M, Martin JD, Martin MR, Vianello F et al (2012) Vascular normalizing doses of antiangiogenic treatment reprogram the immunosuppressive tumor microenvironment and enhance immunotherapy. Proc Natl Acad Sci USA 109(43):17561–17566. https://doi.org/10.1073/pnas.1215397109
30. Zhang J, Li H, Wang X, Qi H, Miao X, Zhang T, Chen G, Wang M (2012) Phage-derived fully human antibody scFv fragment directed against human vascular endothelial growth factor receptor 2 blocked its interaction with VEGF. Biotechnol Prog 28(4):981–989. https://doi.org/10.1002/btpr.1559
31. Xie W, Li D, Zhang J, Li Z, Acheampong DO, He Y, Wang Y, Chen Z, Wang M (2014) Generation and characterization of a novel human IgG1 antibody against vascular endothelial growth factor receptor 2. Cancer Immunol Immunother 63(9):877–888. https://doi.org/10.1007/s00262-014-1560-9
32. Acheampong DO, Tang M, Wang Y, Zhao X, Xie W, Chen Z et al (2017) A novel fusion antibody exhibits antiangiogenic activity and stimulates NK cell-mediated immune surveillance through fused NKG2D ligand. J Immunother 40(3):94–103. https://doi.org/10.1097/CJI.0000000000000157
33. Ferrari de Andrade L, Tay RE, Pan D, Luoma AM, Ito Y, Badrinath S, Tsoucas D, Franz B, May KF Jr, Harvey CJ et al (2018) Antibody-mediated inhibition of MICA and MICB shedding promotes NK cell-driven tumor immunity. Science 359(6383):1537–1542. https://doi.org/10.1126/science.aao0505
34. Wang T, Sun F, Xie W, Tang M, He H, Jia X, Tian X, Wang M, Zhang J (2016) A bispecific protein rG7S-MICA recruits natural killer cells and enhances NKG2D-mediated immunosurveillance against hepatocellular carcinoma. Cancer Lett 372(2):166–178. https://doi.org/10.1016/j.canlet.2016.01.001
35. Stoufer LK, Davies LD, Culpepper D, McFarland BJ (2009) Rational design of enhanced affinity at the MICA-NKG2D interface (134.51). J Immunol 182:134.151–134.151
36. Hodi FS, Lawrence D, Lezcano C, Wu X, Zhou J, Sasada T, Zeng W, Giobbie-Hurder A, Atkins MB, Ibrahim N et al (2014) Bevacizumab plus ipilimumab in patients with metastatic melanoma. Cancer Immunol Res 2(7):632–642. https://doi.org/10.1158/2326-6066.CIR-14-0053
37. Wallin JJ, Bendell JC, Funke R, Sznol M, Korski K, Jones S, Hernandez G, Mier J, He X, Hodi FS et al (2016) Atezolizumab in combination with bevacizumab enhances antigen-specific T-cell migration in metastatic renal cell carcinoma. Nat Commun 7:12624. https://doi.org/10.1038/ncomms12624
38. Ramjiawan RR, Griffioen AW, Duda DG (2017) Anti-angiogenesis for cancer revisited: is there a role for combinations with immunotherapy? Angiogenesis 20(2):185–204. https://doi.org/10.1007/s10456-017-9552-y
39. Krebs P, Barnes MJ, Lampe K, Whitley K, Bahjat KS, Beutler B et al (2009) Nk cell-mediated killing of target cells triggers robust antigen-specific T cell-mediated and humoral responses. Blood 113(26):6593–6602
40. Deng J, Liu X, Rong L, Ni C, Li X, Yang W (2014) Ifnγ-responsiveness of endothelial cells leads to efficient angiostasis in tumours involving down-regulation of dll4. J Pathol 233(2):170–182
41. Lu Y, Yang W, Qin C, Zhang L, Deng J, Liu S et al (2009) Responsiveness of stromal fibroblasts to ifn-γ blocks tumor growth via angiostasis. J Immunol 183(10):6413–6421
42. Khan KA, Kerbel RS (2018) Improving immunotherapy outcomes with anti-angiogenic treatments and vice versa. Nat Rev Clin Oncol 15:310–324